SUSC 13122
18 October 2002 Disk used
ARTICLE IN PRESS
No. of Pages 9, DTD = 4.3.1
SPS-N, Chennai

ELSEVIER

Available online at www.sciencedirect.com
SCIENCE DIRECT®

Surface Science xxx (2002) xxx–xxx

SURFACE SCIENCE

www.elsevier.com/locate/susc

Surface Science Letters

STM images of molecularly and atomically chemisorbed oxygen on silver

F.E. Olsson [a,*], N. Lorente [b], M. Persson [a,*]

[a] Department of Applied Physics, Chalmers/Göteborg University of Technology Physics, S-41296 Göteborg, Sweden
[b] Laboratoire Collisions, Agrégats, Réactivité, UMR 5589, Université Paul Sabatier, 31062 Toulouse Cedex, France

Received 27 May 2002; accepted for publication 28 September 2002

Abstract

We present a theoretical study of scanning tunneling microscopy/microscope (STM) images of two chemisorbed, molecular precursors of O_2 and chemisorbed O on Ag(1 1 0). The electronic structure and the equilibrium geometric structure of these precursors were obtained from density functional calculations and STM images were calculated from the Kohn–Sham wave functions using the Tersoff–Hamann approximation. This study provide a quantitative analysis of molecular contrast versus molecular orientation, tip–surface distance and character of tip orbital. Our calculated STM images are in good agreement with experimental STM images. We explain the large separation between the experimentally observed protrusions compared to the O–O bond distance using the vacuum tails of a model wave function for an anti-bonding state of O_2.

Keywords: Scanning tunneling microscopy; Oxygen; Chemisorption; Silver; Density functional theory

1. Introduction

The interaction of oxygen with an (1 1 0) surface of silver involves several molecularly adsorbed states and may be viewed as a model system for the study of molecular precursors. The chemisorption properties of this system have attracted a lot of attention both from theoretical and experimental studies [1–9]. In a density functional study by Gravil and Bird two chemisorbed molecular precursors of oxygen molecules were identified corresponding to two different orientations of the molecule [8]. This prediction were later confirmed by electron energy loss experiments [4]. These precursors were directly imaged in scanning tunneling microscopy/microscope (STM) experiments by Hahn and coworkers [1,2]. They were able to determine the adsorption site of the molecular precursors by imaging the underlying substrate lattice. Using a functionalized tip, they could also resolve protrusions in the images for one of the molecular precursors that were attributed to an anti-bonding molecular π resonance. These protrusions were used to infer the orientation of the molecular precursors. There is a need to under-

* Corresponding authors. Tel.: +46-31-772-8420; fax: +46-31-772-8426 (F.E. Olsson), fax: +46-31-772-8426 (M. Persson).
E-mail addresses: folsson@fy.chalmers.se (F.E. Olsson), tfymp@fy.chalmers.se (M. Persson).

0039-6028/02/$ - see front matter © 2002 Published by Elsevier Science B.V.
PII: S0039-6028(02)02358-0

stand the nature of these images and what kind of information that can be obtained from them. In particular, when using a functionalized tip, why are protrusions observed in the STM image of only one of the precursors?

Several different theoretical schemes for simulating STM images of chemisorbed molecules on metal surfaces have been proposed [11,12]. A widely used scheme is based on semi-empirical electronic structure calculations using a non-perturbative scattering approach to tunneling. Another scheme that is able to provide a more accurate description of the bonding parameters is based on density functional theory (DFT) and the Tersoff–Hamann approximation for tunneling [13]. The TH approximation gives a simple, physical interpretation in terms of the local density of states (LDOS) at the tip apex and at the Fermi energy. However, the TH approximation is controversial because of its simplified treatment of the STM tip, perturbative character and range of applicability for simulating STM images of isolated adsorbates is not clear. Furthermore, the DFT-TH scheme for simulations of STM images have been limited to high coverages and unrealistically short tip–surface distances [14,15] with some contradictory results. For example, using the DFT-TH scheme Bocquet et al. [16] were unable to obtain a satisfactory representation of STM images for O_2 on Pt(1 1 1) [18], whereas Eichler et al. [17] found a qualitative agreement with the same images using the same scheme. Furthermore, STM image simulations of atomic oxygen on metal surfaces using the DFT-TH scheme have reported both a protrusion [16] and a depression [15], whereas experimental STM images exhibit a depression [12]. Thus it is important to explore the usefulness of the DFT-TH scheme by calculating STM images from isolated adsorbates at appropriate tip–surface distances and at low coverages. Recently, we have shown that the DFT-TH scheme is able to give a good representation of experimental STM images of adsorbed hydrocarbons on a copper surface, obtained using both regular and functionalized tips [10].

In this paper we present density functional calculations of chemisorption parameters and STM images of the two molecular precursors of O_2 and of an O atom on Ag(1 1 0). The constant current STM images were calculated from the Kohn–Sham wave functions using the TH approximation [13]. The electronic structures of the adsorbates were analyzed using electron density differences and density of states projected on atomic orbitals or linear combinations of atomic orbitals, for O and O_2, respectively. Using the vacuum tails of a model molecular wave function, we discuss the large apparent size of the protrusions in the STM images.

2. Method

The density functional calculations of the chemisorbed O_2 molecule and the O atom on Ag(1 1 0) were carried out using the plane wave, pseudopotential code DACAPO [21]. The interaction of the valence electrons with the ion cores were treated using ultra-soft pseudopotentials [22] with a plane-wave energy cutoff of 35 Ry and the exchange and correlation effects were included using the generalized gradient approximation [23]. The calculation of STM images requires a large surface unit cell so the surface was modeled by a slab in supercell geometry with a (4×3) surface unit cell and six layers of Ag atoms and a vacuum region being equivalent to six layers. A smaller (3×2) surface unit cell was used in the analysis of the electronic structure and in the calculation of the potential energy barrier between the two orientations of the O_2 molecules. This barrier was calculated by carrying out a constrained relaxation of the atoms in a series of calculations where the O–O axis is constrained to lie in a plane perpendicular to the surface with different angles with respect to a symmetry plane of the surface. We used 16 k-points in the surface Brillouin zones (SBZ) of the small and large super cells. The equilibrium geometry were determined by relaxing the O positions and the three outermost Ag layers whereas the remaining Ag layers were fixed at their calculated bulk positions.

The STM images were calculated using the Tersoff and Hamann (TH) approximation for tunneling in an STM junction [13]. At zero temperature and low bias voltage, V, the differential

tunneling conductance, dI/dV is in this approximation proportional to the LDOS at the tip apex, $\mathbf{r}_0$, and at the Fermi energy, ϵ_F, which is given by,

$$\rho(\mathbf{r}_0;\epsilon_F) = \sum_{n\mathbf{k}} |\psi_{n\mathbf{k}}(\mathbf{r}_0)|^2 \delta(\epsilon_{n\mathbf{k}} - \epsilon_F). \quad (1)$$

Here $\psi_{n\mathbf{k}}(\mathbf{r})$ is a Kohn–Sham wave function of the adsorbate-covered surface with energy $\epsilon_{n\mathbf{k}}$, band index n and wave vector $\mathbf{k}$ in the SBZ. The TH result for dI/dV is based on the s-wave approximation for the tip. For a p_z-wave approximation for the tip, dI/dV is proportional to an analogous quantity to the LDOS in Eq. (1) obtained by replacing $\psi_{n\mathbf{k}}(\mathbf{r}_0)$ with $\partial\psi_{n\mathbf{k}}(\mathbf{r}_0)/\partial z$ [19]. The constant-current STM images and profiles correspond to topographical images and profiles of constant $\rho(\mathbf{r}_0;\epsilon_F)$, given by Eq. (1), and will be referred to as LDOS images and profiles, respectively. Before presenting and discussing these results, we need first to present and discuss the results for the geometric and electronic structure of the adsorbates.

3. Chemisorption parameters

We have considered the same configurations for the two molecular precursors and the atom as done in the DFT investigation by Gravil et al. [8]. Our results for bonding parameters are in good agreement with their results considering the use of different pseudopotentials. In particular, the use of ultra-soft pseudopotentials for oxygen is delicate with special needs in handling the core electrons [24]. The two molecular configurations correspond to the O_2 molecule being adsorbed in the hollow site either with the O–O axis in the [0 0 1] or in the [1 $\bar{1}$ 0] directions, as shown in Fig. 1(a) and (b), respectively. These two molecular precursors will henceforth be referred to as $O_{2[0\,0\,1]}$ and $O_{2[1\,\bar{1}\,0]}$, respectively. The O atom is adsorbed in the fourfold hollow site, as shown in Fig. 1(c).

The bonding distances for the two molecular orientations are somewhat different but the energetics are very similar. The O–O bond distance is 1.39 Å for $O_{2[0\,0\,1]}$ which is 0.03 Å smaller than for $O_{2[1\,\bar{1}\,0]}$. The equilibrium height of the molecule above the surface plane is about 1.33 Å for $O_{2[0\,0\,1]}$, which is 0.19 Å higher than for $O_{2[1\,\bar{1}\,0]}$. This difference in adsorption height is simply a geometrical effect of keeping the O–Ag bond distance more or less the same for the two molecular precursors. Our calculated chemisorption energy is 0.37 eV for both orientations, which is consistent with the experimental observation that both precursors are observed at the same surface temperature. We found that the potential energy barrier between the two orientations is 0.45 eV and is located at an angle of 45° for the O–O axis with respect to the [0 0 1] direction. This result suggest that the molecule will rather desorb than switch orientation when elevating the temperature. Note that Gravil and Bird only estimated the location of this barrier and hence its magnitude.

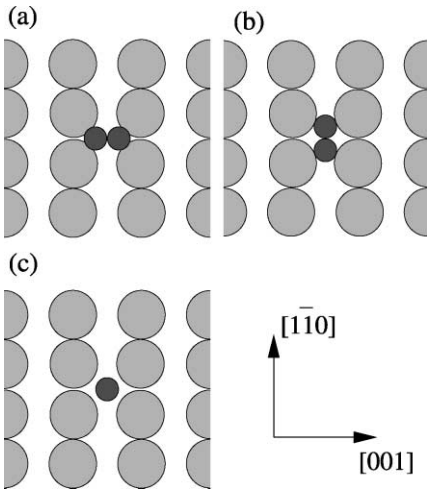

Fig. 1. Surface unit cell and chemisorption geometries for O_2 (a,b) and O (c) on Ag(1 1 0). The molecular axis of O_2 is along the [0 0 1] direction ($O_{2[0\,0\,1]}$) in (a) and along the [1 $\bar{1}$ 0] direction ($O_{2[1\,\bar{1}\,0]}$) in (b). Large and small circles represent Ag and O atoms, respectively.

As expected for an open shell atom, the O atom forms a strong chemisorption bond with a metal surface such as Ag(1 1 0). In the fourfold hollow site, the atom-surface distance is 0.57 Å and the adsorption energy is 3.50 eV.

The nature of the electronic states of the chemisorbed molecular precursors and atom is revealed by the PDOS on the bonding and antibonding π orbitals of O_2 and the PDOS on the p

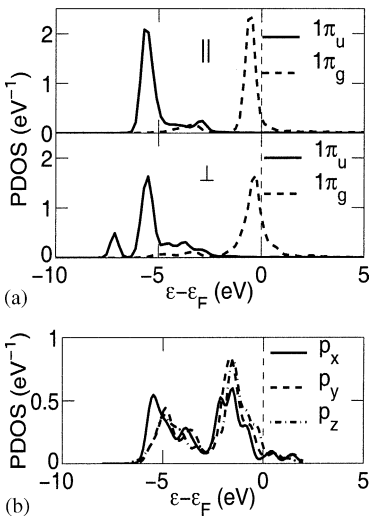

Fig. 2. Calculated projected density of states (PDOS) for $O_{2[1\bar{1}0]}$ (a) and O (b), chemisorbed on Ag(1 1 0). (a) The density of states are projected on linear combination of atomic p orbitals modeling the bonding and anti-bonding π molecular orbitals of O_2 oriented parallel to the surface in top panel ($1\pi_g^{\parallel}$ and $1\pi_u^{\parallel}$) or perpendicular to the surface in lower panel ($1\pi_g^{\perp}$ and $1\pi_u^{\perp}$). (b) The density of states are projected on atomic p orbitals.

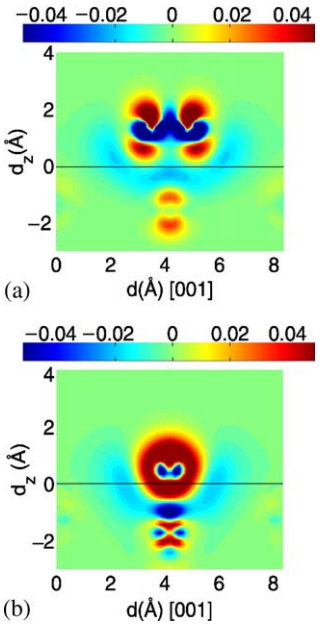

Fig. 3. Density difference contours of (a) $O_{2[0\,0\,1]}$ and (b) O on Ag(1 1 0). The contour planes are perpendicular to the surface (d_z) and along the [0 0 1] direction, through the adsorbate. Density differences for values larger then 0.05 and less than −0.05 electrons/Å^3 have been truncated. $d_z = 0$ corresponds to the position of the first atomic surface layer. The calculations were carried out in a 3 × 2 surface unit cell with 16 *k*-points in the SBZ.

orbitals of O, respectively. The PDOS for $O_{2[1\bar{1}0]}$ and $O_{2[0\,0\,1]}$ are very similar and only the PDOS for $O_{2[1\bar{1}0]}$ is shown in Fig 2(a). Around the Fermi level and above the energy range of the d band, the PDOS is dominated by narrow molecular resonances derived from anti-bonding molecular states $1\pi_g$. The resonance that is derived from the $1\pi_g^{\parallel}$ state where the atomic p states are parallel to the surface is almost filled, whereas the resonance that derives from the $1\pi_g^{\perp}$ where the atomic p states are perpendicular to the surface is partially filled. The net donation of more than one electron to the anti-bonding π orbitals of the O_2 molecule results in a weakening of the intra-molecular bond and an elongation of its bond distance with about 0.15 Å upon adsorption. As shown in Fig. 2(b), the p subshell of the O atom hybridizes strongly with the d band and is almost completely filled upon chemisorption, indicating an O^{2-} charged state.

The filling and the characteristic spatial dependence of the anti-bonding π states of O_2 and the p states of O upon chemisorption is directly revealed in the contours of electron density differences, $\delta n(\vec{r})$, in Fig. 3. In both cases, the contours of $\delta n(\vec{r})$ show also that the d states of the nearest neighboring atom in the second layer of Ag are participating in the chemisorption bond. Another common feature that is present in the density difference contours for both O_2 and O is the region of electron density depletion in the vicinity of the adsorbate. This depletion is due to a decrease in the free-electron like density of metal states and is associated with the two related effects: (1) electron transfer from the free-electron like states into the π or p states of O_2 and O, respectively, (2) screening of the negative charge transferred into the adsorbate states by the free-electron like metal states.

4. Simulated STM images

Based on our results for the geometric and electronic structure we can now make a comprehensible presentation and discussion of the results for the LDOS images and profiles of $O_{2[1\bar{1}0]}$ and $O_{2[001]}$ and the chemisorbed O atom shown in Figs. 4–6, respectively. A common feature of all the LDOS images and profiles is the wide depression, which extends about 4–5 Å from the center of the adsorbate. A characteristic feature of the molecular LDOS images and profiles are the two protrusions along the molecular axis of O_2, which are much more pronounced for $O_{2[1\bar{1}0]}$ than for $O_{2[001]}$. These two features are now discussed in turn.

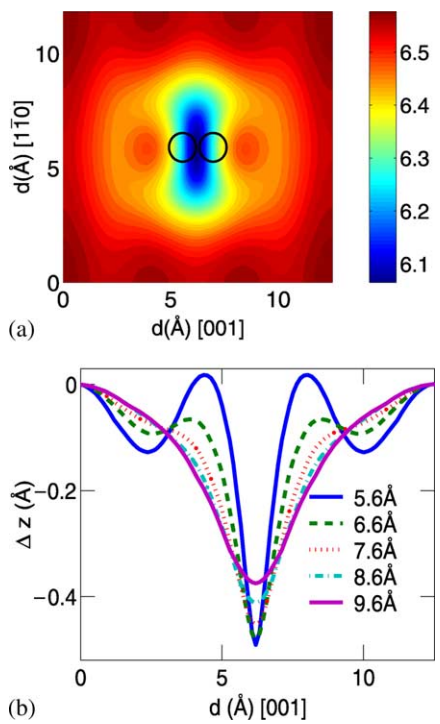

Fig. 4. Calculated LDOS (a) images and (b) profiles along the molecular axis for $O_{2[001]}$ on Ag(1 1 0). $\Delta z = 0$ corresponds to an initial tip–surface distance of $z_0 = 5.6$, 6.6, 7.6, 8.6, and 9.6 Å for the profiles and to 6.6 Å for the image. The geometric configuration of $O_{2[001]}$ is indicated by the two black circles in the LDOS image. The discrete spectrum of Kohn–Sham states was broadened by a Gaussian approximation to the delta function in Eq. (1) using a width of $\sigma = 0.25$ eV. The calculations were carried out in a 4×3 surface unit cell with 16 k-points in the SBZ.

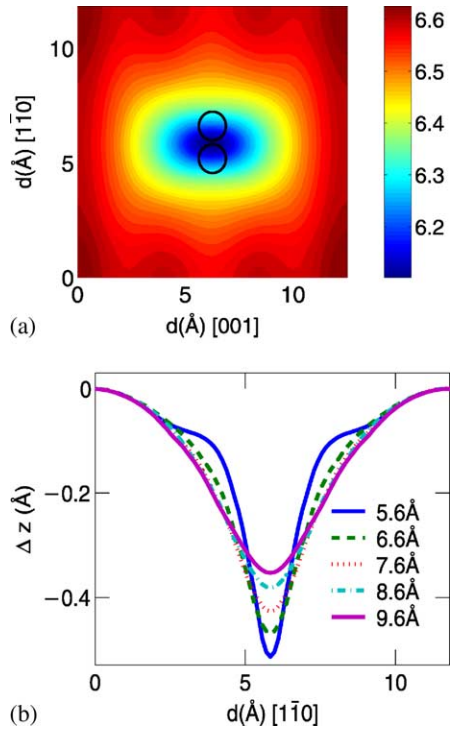

Fig. 5. Calculated LDOS (a) images and (b) profiles along the molecular axis for $O_{2[1\bar{1}0]}$ on Ag(1 1 0). $\Delta z = 0$ corresponds to an initial tip–surface distance of $z_0 = 5.6$, 6.6, 7.6, 8.6, and 9.6 Å for the profiles and to 6.6 Å for the image. The configuration of $O_{2[1\bar{1}0]}$ is indicated by the two black circles in the LDOS image. Same supercell, k-points and σ, as in Fig. 4.

The wide depression in the LDOS images is associated with the decrease of metal free-electron like density in the vicinity of the adsorbate, due to screening of of the electronegative adsorbate. This interpretation is corroborated by two findings: (1) the size of the depression in the LDOS images are about the same as the electron depletion region of the electron density difference, as shown in Fig. 3, (2) the development of the depression with increasing tip–surface distances is moderate which shows that these states has a decay into the vacuum which is similar to that of the clean Ag(1 1 0), that is, mainly free-electron like.

The two protrusions in the LDOS images of $O_{2[1\bar{1}0]}$ and $O_{2[001]}$ are in both cases associated with the $1\pi_g^{\perp}$ derived resonance that has a large contribution at the Fermi level and two perpendicular lobes. In the LDOS image these lobes will give rise

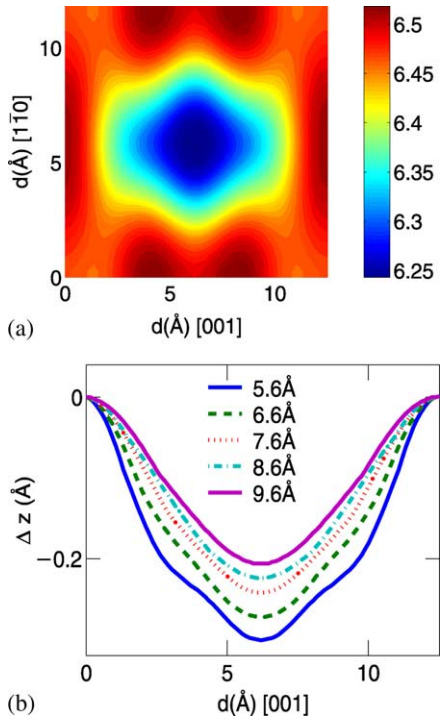

Fig. 6. Calculated LDOS (a) images and (b) profiles along the [0 0 1] direction of O on Ag(1 1 0). $\Delta z = 0$ corresponds to an initial tip–surface distance of $z_0 = 5.6$, 6.6, 7.6, 8.6, 9.6 Å for the profiles and 6.6 Å for the image. The O is located in the center of the LDOS image. Same supercell, k-points and σ, as in Fig. 4.

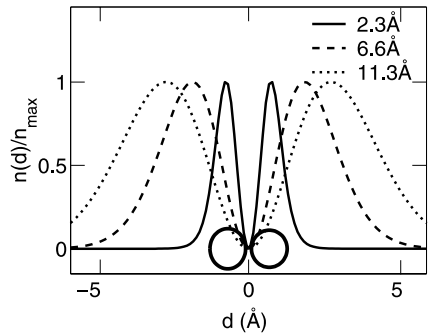

Fig. 7. Calculated densities of a single $1\pi_g^{\perp}$ model wave function along a line through the molecular axis at different tip–surface distances of $z_0 = 2.3$, 6.6, and 11.3 Å. The positions of the O atoms are indicated by the open circles. The densities, $n(d)$, are constructed using Eq. (2), and are normalized to their maximum value, n_{max}, along the line.

to two protrusions with a relatively large separation, which can be understood using a simple model for the contribution of the $1\pi_g^{\perp}$ derived resonance at the tip apex. This contribution is modeled by the density $n_{1\pi_g^{\perp}}(\mathbf{r}_0)$ of a model wave function obtained from an anti-symmetric combination of the vacuum tails of two states with p_z symmetry as,

$$n_{1\pi_g^{\perp}}(\mathbf{r}_0) = \frac{1}{2}\left|\frac{\partial}{\partial z}\psi_s(\mathbf{r}_0 - \mathbf{r}_1) - \frac{\partial}{\partial z}\psi_s(\mathbf{r}_0 - \mathbf{r}_2)\right|^2 \qquad (2)$$

where $\mathbf{r}_0$ is the position of the tip apex, $\mathbf{r}_{1,2}$ are the positions of the two O atoms, z is the direction perpendicular to molecular defined by the p_z atomic orbitals and $\psi_s(\mathbf{r}) \propto e^{-\kappa r}/\kappa r$ [19], where the decay constant $\kappa = \sqrt{2m_e\phi}/\hbar \approx 1.1$ Å^{-1} is determined by the calculated work function ϕ of about 4.3 eV. The profiles of $n_{1\pi_g^{\perp}}(\mathbf{r}_0)$, shown in Fig. 7, have two protrusions separated by distance, d_p, that varies strongly with the tip–surface distance, z_0. At close distance it converges to O–O bond distance, $d_{O\text{–}O}$, of about 1.4 Å whereas at $z_0 = 6.6$ Å, $d_p = 3.7$ Å, which is comparable to $d_p = 4.6$ Å in the LDOS image at the same tip–surface distance, shown in Fig. 4. For large tip–molecule distances, z_m, $\kappa z_m \gg 1$ and $z_m/d_{O\text{–}O} \gg 1$, the variation of d_p with z_m has a simple analytic form, $d_p \sim 2\sqrt{z_m/\kappa}$, that can be obtained from the asymptotic behavior of $n_{1\pi_g^{\perp}}(\mathbf{r}_0) \sim |(\partial^2/\partial z\partial x)\psi_s \times (\mathbf{r}_0 - (\mathbf{r}_1 + \mathbf{r}_2)/2))|^2$, where x is the coordinate along the molecular axis. For instance, at $z_m = 5.3$ Å, corresponding to $z_0 = 6.6$ Å, $2\sqrt{z_m/\kappa} \sim 4.4$ Å.

There are primarily two reasons why the contribution from the $1\pi_g^{\perp}$ resonance dominates over the contribution from the $1\pi_g^{\parallel}$ contribution to the LDOS image. First, the PDOS in the former state is larger at the Fermi energy than the latter state, as shown in Fig. 2. Second, the wave function of the $1\pi_g^{\perp}$ gives a relatively larger contribution in the vacuum region than the wave function of the $1\pi_g^{\parallel}$. This effect can be shown directly from the asymptotic behavior of the model wave functions of these states, using Eq. (2) for $1\pi_g^{\perp}$ and a similar construction using p_y model wave functions for $1\pi_g^{\parallel}$, see Ref. [19]. For large κz_m and $z_m/d_{O\text{–}O}$ the ratio between the maximum value of the model densities is given by,

$$\frac{n_{1\pi_g^{\parallel}}}{n_{1\pi_g^{\perp}}} = \left(\frac{y}{z_m}\right)^2 \quad (3)$$

The maximum value of $n_{1\pi_g^{\perp}}(\mathbf{r}_0)$ occurs for $y \sim \sqrt{2z_m/\kappa}$ and its contribution to the LDOS is $2/\kappa z_m$ relative to $n_{1\pi_g^{\parallel}}(\mathbf{r}_0)$. At $z_m = 5.3$ and 10 Å, this factor is about 3 and 5, respectively.

We argue that the more pronounced protrusions in the LDOS image for $O_{2[0\,0\,1]}$ than for $O_{2[1\,\bar{1}\,0]}$ is simply a consequence of the differences in the adsorption height. The difference in the strengths of the protrusions is not simply a consequence of differences in the interaction of the $1\pi_g^{\perp}$ state with the metal states because of two findings: (1) the corresponding PDOS for the two molecular precursors are almost indistinguishable around the Fermi level (2) the calculated adsorption energy, which is a measure of the interaction strength, is the same for the two configurations. However, the closer distance of $O_{2[1\,\bar{1}\,0]}$ to the surface than $O_{2[0\,0\,1]}$ suggests that the contribution from the resonance state derived from the $1\pi_g^{\perp}$ state to the LDOS is smaller relative to the contribution from metal states for $O_{2[1\,\bar{1}\,0]}$ than for $O_{2[0\,0\,1]}$. Note that the correspondence between the corrugation of an LDOS image and the molecule–surface distance is non-linear. The corrugations of the LDOS profiles at 5.6 Å for $O_{2[1\,\bar{1}\,0]}$ and at 7.6 Å for $O_{2[0\,0\,1]}$ are similar as shown in Figs. 4 and 5. Thus, to keep the same corrugation of the LDOS image for an outward shift of the molecule of 0.2 Å we need to increase z_0 by about 2 Å at 5.6 Å.

In our calculated LDOS images of adsorbed O we find only a wide depression and no protrusion, as shown in Fig. 6. The absence of any protrusion in this case is understood from the electronic structure and adsorption distance of O on Ag(1 1 0). The contributions of the resonances derived from the p subshell of states of the O atom to the PDOS at the Fermi level are small. Furthermore, the contribution to LDOS from tunneling through metal-like states is favored over the contribution from tunneling through adsorbate-like states by the close adsorption distance of the O atom to the first layer of substrate atoms.

Our calculated LDOS images for $O_{2[0\,0\,1]}$ and $O_{2[1\,\bar{1}\,0]}$ are in near-quantitative agreement with the experimental STM images by Hahn and coworkers [1,2]. Using a functionalized tip that was formed by a transfer of a single CO molecule from the surface to the tip, they were able to enhance the resolution of the STM images of the molecular precursors and to resolve two protrusions in the STM image for one of the molecular precursors. The observed spatial extension and depth of the depressions in the images for two molecular precursors and the observed height and distance between the two protrusions in the image $O_{2[0\,0\,1]}$ are nicely reproduced by our calculated LDOS images at $z_0 \approx 7$ Å. For STM images obtained with a regular tip the experimental STM images of the two molecular precursors and chemisorbed O are in good agreement with the calculated LDOS images at $z_0 \approx 9$ Å. Also Zambelli et al. [6] have measured STM images of O_2 chemisorbed on Ag(1 1 0), where O_2 is imaged as a symmetric depression similar to the regular tip STM images of $O_{2[1\,\bar{1}\,0]}$ and $O_{2[0\,0\,1]}$ by Hahn and coworkers. Note that at large tip–surface distances only a large uncharacteristic depression appear in the LDOS images and profiles for the chemisorbed molecule and atom. In particular, this makes it difficult to discriminate between their chemical identities from STM images obtained using a regular tip. Furthermore, the elongation of the depression is perpendicular to the molecular axis, which shows that the orientation of the molecule cannot be inferred simply from the shape of its STM image.

We have simulated STM images using a p_z approximation of the tip. One could argue that this model should represent better a CO-functionalized tip considering the electronic structure of a CO molecule, where the CO 5σ orbital is expected to give the main contribution [16]. However, we find that the simulated STM images using the p_z-wave approximation gives essentially the same images as the s-wave approximation at a tip–surface distance that is about 1 Å larger than for the s-wave approximation, as shown in Fig. 8.

5. Summary

We have carried out density functional calculations of STM images of two molecular precur-

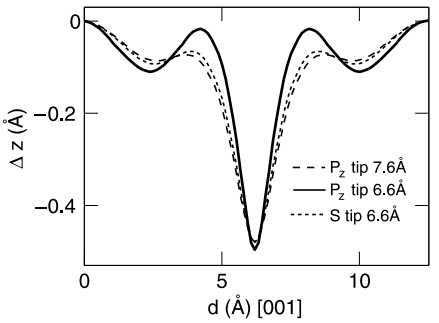

Fig. 8. Simulated STM profiles for $O_{2[001]}$ along the [0 0 1] using an s-wave tip (dashed line), corresponding to LDOS image of Fig. 4, and a p_z-wave tip (solid line). $\Delta z = 0$ corresponds to $z_0 = 6.6$ or 7.6 Å, as indicated in the figure. Same supercell, k-points and σ, as in Fig. 4.

sors of O_2 and O chemisorbed on Ag(1 1 0) using the TH approximation for tunneling. We find a good agreement between experimental STM images of the molecular precursors obtained using both regular and functionalized tips and chemisorbed O obtained using a regular tip and our LDOS images evaluated at appropriate tip–surface distances. This shows that density functional calculations together with the TH approximation is a useful scheme for simulating STM images of single adsorbates. At large tip–surface distances the LDOS images are similar so that STM images from regular tips do not simply discriminate between chemisorbed O and O_2. Our analysis of the calculated LDOS images shows that the observed protrusions derive from tunneling through a single molecular resonance state of $O_{2[001]}$ introduced by the $1\pi_g^{\perp}$ molecular orbital of O_2. The strengths of these protrusions are drastically reduced for the $O_{2[1\bar{1}0]}$ compared to $O_{2[001]}$ because the shorter molecule–surface distance for $O_{2[1\bar{1}0]}$ than for $O_{2[001]}$ decreases the tunneling through the molecule relative to the substrate. We show that the large apparent separation between the two protrusions compared to the O–O bond distance is caused by the behavior of the vacuum tails of the wave functions associated with the resonance derived from $1\pi_g^{\perp}$ state.

6. Uncited reference

[20]

Acknowledgements

We are grateful for the support provided by the Swedish Research Council (MP and FO); the Institute of Surface and Interface Science, University of California, Irvine, (MP); the National Science Foundation Grant no. DMR–0102887 (MP). Allocations of computer resources at the center of parallel computing in Stockholm, the consortium for heavy computing at Chalmers, the centre de calcul Midi-Pyrénées (NL), and le Centre d'Informatique National de l'Enseignement Supérieur (NL) are also gratefully acknowledged.

References

[1] J.R. Hahn, H.J. Lee, W. Ho, Phys. Rev. Lett. 85 (2000) 1914.
[2] J.R. Hahn, W. Ho, Phys. Rev. Lett. 87 (2001) 196102.
[3] J.R. Hahn, W. Ho, Phys. Rev. Lett. 87 (2001) 166102.
[4] F. Bartolucci, R. Franchy, J.C. Barnard, R.E. Palmer, Phys. Rev. Lett. 80 (1998) 66.
[5] J.V. Barth, T. Zambelli, J. Wintterlin, G. Ertl, Surf. Sci. 270 (1997) 152.
[6] T. Zambelli, J.V. Barth, J. Wintterlin, J. Phys.: Condens. Matter 14 (2002) 4241.
[7] D.A. Outka, J. Stöhr, W. Jark, P. Stevens, J. Solomon, R.J. Madix, Phys. Rev. B 35 (1987) 4119.
[8] P.A. Gravil, D.M. Bird, J.A. White, Phys. Rev. Lett. 77 (1996) 3933.
[9] V.I. Pazzi, P.H.T. Philipsen, E.J. Baerends, G.F. Tantardini, Surf. Sci. 443 (1999) 1.
[10] F.E. Olsson, N. Lorente, M. Persson, L.J. Lauhon, W. Ho, J. Phys. Chem. B 106 (2002) 8161.
[11] A.S. Foster, W.A. Hofer, A.L. Schluger, Curr. Opin. Solid State Mater. Sci. 5 (2001) 427.
[12] P. Sautet, Chem. Rev. 97 (1997) 1097.
[13] J. Tersoff, D.R. Hamann, Phys. Rev. Lett. 50 (1983) 1998.
[14] S. Helveg, H.T. Lorensen, S. Horch, E. Lægsgaard, I. Stensgaard, K.W. Jacobsen, J.K. Nørskov, F. Besenbacher, Surf. Sci. 430 (1999) L533.
[15] J. Jacobsen, B. Hammer, K.W. Jacobsen, J.K. Nørskov, Phys. Rev. B 520 (1995) 14954.
[16] M.-L. Bocquet, J. Cerda, P. Sautet, Phys. Rev. B 59 (1999) 15437.
[17] A. Eichler, F. Mittendorfer, J. Hafner, Phys. Rev. B 62 (2000) 4744.

[18] B. Stipe, M.A. Rezaei, W. Ho, Science 279 (1998) 1907.
[19] C.J. Chen, Introduction to Scanning Tunneling Microscopy, Oxford University Press, New York, 1993.
[20] W.A. Hofer, A.J. Fisher, R.A. Wolkow, P. Grütter, Phys. Rev. Lett. 87 (2001) 236104-1.
[21] L. Hansen et al., Dacapo-1.30, Center for Atomic Scale Materials Physics (CAMP), Denmark Technical University.
[22] D. Vanderbilt, Phys. Rev. B 41 (1990) 7892.
[23] J.P. Perdew, J.A. Chevary, S.H. Vosko, K.A. Jackson, M.R. Pederson, D.J. Singh, D. Fiolhais, Phys. Rev. B 46 (1992) 6671.
[24] B. Hammer, L.B. Hansen, J.K. Nørskov, Phys. Rev. B 59 (1999) 7413.